Density Functional Study of Ribose and Deoxyribose Chemical Shifts

Annick P. Dejaegere

Groupe RMN-UPR 9003, Ecole Supérieure de Biotechnologie de Strasbourg, 67400 Illkirch, France, and Lab. de Chimie Biophysique, ISIS-UPRESA-7006 CNRS, rue B. Pascal, 67000 Strasbourg, France

David A. Case*

Department of Molecular Biology, The Scripps Research Institute, La Jolla, California 92307

Received: January 28, 1998; In Final Form: April 29, 1998

Density functional chemical shielding calculations are reported for methyl β-D-2-deoxyribofuranoside and for methyl β-D-ribofuranoside, models for the deoxyribose and ribose sugars in nucleic acids. The variation of the chemical shielding as a function of the sugar ring conformation is reported, as well as the influence of the ring conformation on the chemical shift anisotropy. The calculated chemical shieldings are sensitive to the puckering of the sugar ring. The value of the exocyclic torsion angles, particularly γ(O5′−C5′−C4′−C3′), are also found to influence the chemical shielding of the ring atoms. The chemical shielding of the C3′ carbon is the most sensitive to the sugar ring pucker, with a variation of 10 ppm between the C3′ endo and C2′ endo conformations. H3′ and H4′ hydrogen shieldings vary by 0.4−0.6 ppm between the C3′ endo and C2′ endo conformations. Chemical shift anisotropies at C1′ and C3′ are strongly influenced by sugar pucker. Our results agree well with experimentally reported values of chemical shifts in methyl β-D-2-deoxyribofuranoside and methyl β-D-ribofuranoside. They also agree with observed solid-state correlations between C3′ and C5′ chemical shift and sugar ring pucker and point to new methods for the analysis of nucleic acid conformation in solution.

1. Introduction

Advances in NMR instrumentation and methodology have now made it possible to make site-specific chemical shift assignments for a large number of proteins and nucleic acids. It has been known for a long time that chemical shifts are sensitive to details of molecular structures, but models for relating the shifts to structure have not been available, so that the major source of data for NMR structure determination has been the nuclear Overhauser effect (NOE) and spin−spin coupling constants. There is increasing evidence of correlations between 3-D structures and chemical shift trends.[1−7] The large number of NMR structures available has made possible the development of semiempirical theories for chemical shift dispersion that allow the calculations of proton chemical shifts in proteins.[8−12]

Quantum chemical calculations of chemical shifts have also significantly progressed in the last years.[13−19] Calculations of ^{13}C shielding in model peptides and small molecules in the gas phase have been used to trace the dependence of carbon peptide shielding on ϕ and ψ backbone angles.[20−22] Another use of quantum shift calculations is in the development and parametrization of physical models of environmental shift effects; this can be done by studying small molecules in simple geometries and combinations, so that different contributions to the shift and their behavior with conformational change can be isolated and quantitated.[23]

Less attention has been paid to shift distributions in nucleic acids. A thorough theoretical study of protons, nitrogen and carbon chemical shift trends in nucleic acids was performed some years ago by Giessner-Prettre and Pullman.[24] Owing to limitations in the computational power available at the time, these quantum calculations were performed using semiempirical or minimal basis set ab initio methods. The agreement between these theoretical studies and the experimental data available at the time was variable. In some cases qualitative trends in the observed shifts could not be successfully predicted. In view of the significant advances in the quantum methods available for calculating chemical shifts, as well as in the vastly increased number of nucleic acids experimentally studied by NMR,[25−27] it is useful to perform new quantum calculations on nucleic acids components.

In this work, density functional quantum calculations are used to investigate the relationship between sugar conformation and chemical shift in methyl β-D-2-deoxyribofuranoside (Figure 1.1) and methyl β-D-ribofuranoside (Figure 1.2). The conformational dependence of ^{13}C and ^{1}H shifts is examined, and a comparison with experimental results is presented.

2. Methods

2.1. Structures. Chemical shifts of ^{1}H and ^{13}C were calculated by density functional methods for methyl β-D-2-deoxyribofuranoside (**1**) and for methyl β-D-ribofuranoside (**2**). Ab initio geometry optimizations were conducted with Gaussian 94,[28] using both density functional and Hartree−Fock methods. The density functional optimizations used the Becke exchange functional[29] and the Perdew−Wang-91 correlation functional[30] with a 6-31G* basis set.[31] Hartree−Fock optimizations using the 6-31G* basis set were also performed as well as Hartree−Fock and MP2 optimizations with a 6-31G** basis, which includes polarization functions on hydrogen atoms.[31] Different sets of constraints were applied on the dihedral angles internal to the ring in order fix the pseudorotation angle. In one set of

S1089-5639(98)00926-8 CCC: $15.00
Published on Web 06/17/1998

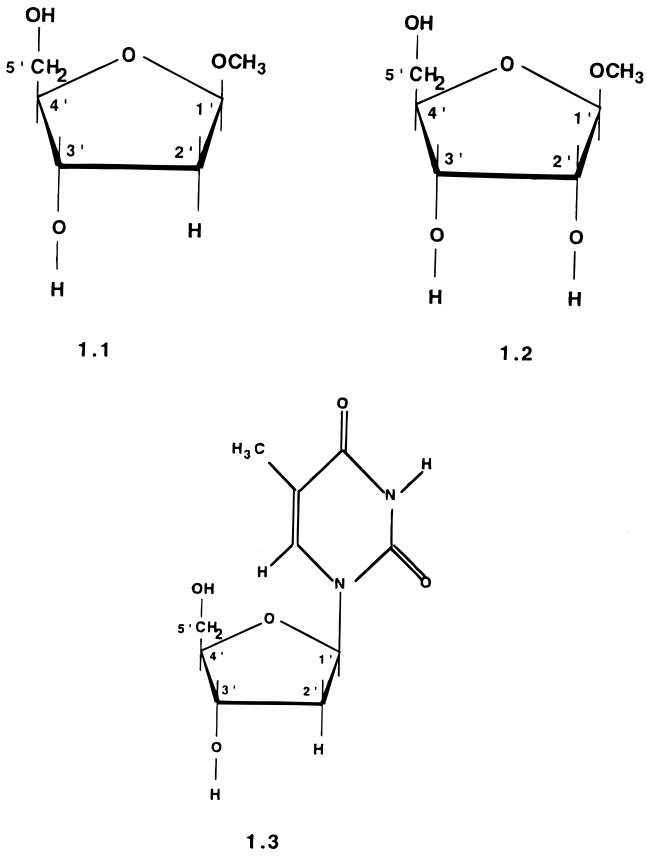

Figure 1. Structure of the model compounds used in the study: **1.1**, methyl β-D-2-deoxyribofuranoside; **1.2**, methyl β-D-ribofuranoside; **1.3** deoxythymidine.

calculations, four dihedrals were constrained as

$$\nu_i = \tau_m \cos(P + 144(i-2)) \quad i=1, 2, 3, 4 \qquad (1)$$

where τ_m is the maximum torsion and P is the desired pseudorotation phase angle.[32] The five dihedrals internal to the ring are

$$\nu_0 = C_{4'}-O_{4'}-C_{1'}-C_{2'}$$

$$\nu_1 = O_{4'}-C_{1'}-C_{2'}-C_{3'}$$

$$\nu_2 = C_{1'}-C_{2'}-C_{3'}-C_{4'}$$

$$\nu_3 = C_{2'}-C_{3'}-C_{4'}-O_{4'}$$

$$\nu_4 = C_{3'}-C_{4'}-O_{4'}-C_{1'}$$

They are linked by the relation[32]

$$\nu_0 + \nu_1 + \nu_2 + \nu_3 + \nu_4 = 0 \qquad (2)$$

The maximum torsion τ_m was set to 38.0°, and structures were generated between $P = 0$ and $P = 360$ at 15° increments for the deoxyribose and at 30° increments for the ribose. The dihedrals ν_i ($i = 1, 2, 3, 4$) were constrained during the geometry optimization with all other parameters optimized. P and τ_m were recalculated after each geometry optimization, and they were always within 1° of the values used as input in eq 1. In a second set of calculations, geometry optimizations with just one dihedral (ν_3) constrained were performed. These allow the sugar pucker amplitude to vary, but the resulting pseudorotation phase was not always that predicted from eq 1. The various sets of calculations performed are summarized in Table 1.

TABLE 1: Description of the ab Initio Methods and Dihedral Angle Constraints

ab initio method[a]	constraints applied[b]	deoxy[c]	ribose[a]
BPW91/6-31G*	$\nu1$, $\nu2$, $\nu3$, $\nu4$	D1	R1
BPW91/6-31G*	$\nu3$	D2	
HF/6-31G*	$\nu3$	D3	
HF/6-31G**		D4	R4
MP2/6-31G**		D5	

[a] See ref 59 and the method section for a complete description. [b] The constraints are applied on the dihedral angles internal to the ring in order fix the pseudorotation angle. [c] The letter codes D1, ..., D5 and R1, R4 are used to represent the different sets of results. For the ribose, only the calculations corresponding to R1 and R4 were performed.

In addition to the pseudorotation angle P, the model sugars **1** and **2** contain several other torsion angles for which different conformers are possible: H−O5′−C5′−C4′ (β); O5′−C5′−C4′−C3′ (γ); H−O3′−C3′−C4′ (ϵ); O4′−C1′−O1′−C (χ; the Greek letters refer to the corresponding equivalent in nucleic acid nomenclature[32]). For all the structures considered, the values of the exocyclic torsion are $45° < \beta < 60°$; $40° < \gamma < 65°$; $50° < \epsilon < 65°$; $-75° < \chi < -65°$; except for **2** where ϵ adopts a range of conformations between 40° and 150° as a function of P. The value of the dihedral H−O5′−C5′−C4′ (β) in the range 45°−60° places the HO5′ above the O4′, in a position to form an hydrogen bond. While this is the most favored conformation of the model sugar compounds in the gas phase, it does not correspond to the value of β most frequently observed in nucleic acids ($\beta = 180°$).[33]

A recent statistical survey of the structure of sugar and phosphate constituents of nucleic acids[33] showed that the most frequently encountered values of the other exocyclic dihedral angles are: $\gamma = 52.5°$(with minor population of $\gamma = 293°$ and $\gamma = 179°$); $\epsilon = 214°$; $\chi = 230°$ (anti) or 60° (syn). It was beyond the scope of this work to generate structures with all possible combinations of exocyclic torsion angles, but we did use the D1 set of structures to modify the exocyclic torsion angles (without reoptimizing the ring geometries) to the following values $\beta = \epsilon = 180°$, γ unmodified; $\beta = \epsilon = 180°$, $\gamma = -60°$; $\beta = \gamma = \epsilon = 180°$. Additional geometry optimizations with β constrained to 180° were also performed on sets D4 and R4. These calculations showed that the values of β and ϵ do not significantly influence the shielding of the model sugar, while γ has a marked influence on shielding (see below). The glycosidic torsion (χ) was not modified from its optimized value in set D1. Studies of the influence of the glycosidic torsion on the shielding will be performed on model nucleosides, rather than on the substituted sugars considered here.

Chemical shifts were also calculated on deoxythymidine. The geometry was optimized at the BPW91/6-31G* level.[28] The glycosidic torsion was chosen anti ($180° < \chi < 270°$). The optimized value for χ was correlated with the sugar pucker, with χ close to −160° for C3′ endo conformations and close to −125° for C2′ endo.[32] For $P = 300°$, χ fell in the high-anti range ($\chi = -80°$). The sugar pucker was maintained by constraining the dihedral angles ν_i ($i = 1, 2, 3, 4$) as described above. The exocyclic torsion angles β, γ, and ϵ were in the range $175° < \beta < 185°$; $35° < \gamma < 55°$; $50° < \epsilon < 70°$ (the only exceptions were the structures with $P = 240°$, where $\gamma = 16°$ and $P = 270°$ where $\gamma = -3°$).

2.2. Chemical Shift Calculations. Shielding tensors were computed using the *deMon* program, which combines density

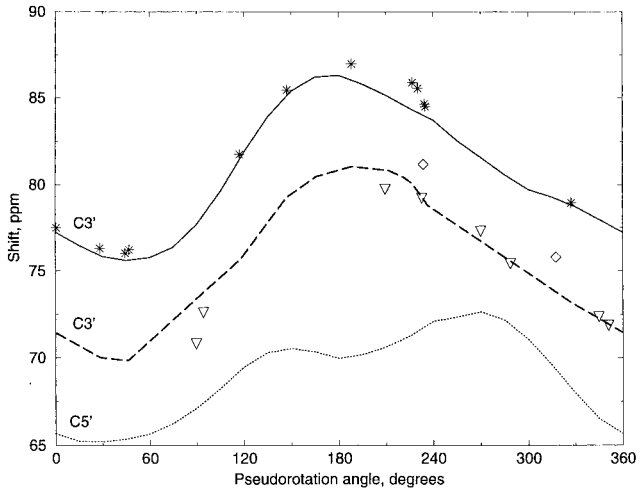

Figure 2. Calculated C3′ and C5′ chemical shifts for the model deoxyribose (Figure 1.1) as a function of the pseudorotation phase *P*. The chemical shift is obtained by subtracting the isotropic *deMon* shielding calculated for C3′ and C5′ from the reference isotropic shielding of 182.05 calculated for C in TMS. The C3′ shifts are calculated as described in section 2.2 for a series of different structures: (solid line) structures obtained at the BPW91/6-31G* level with four dihedral constraints (D1 set, with exocyclic torsions angles $\beta = 60°$; $\epsilon = 60°$; $\gamma = 60°$); (*) BPW91/6-31G*; one dihedral constraint (D2 set); (dashed line) HF/6-31G*, one (D3 set); (▽) HF/6-31G**, full optimization (D4 set); (◇) MP2/6-31G**, full optimization. The C5′ shifts (dotted line) are from the D1 set, with exocyclic torsions angles $\beta = \epsilon = 180°$; $\gamma = 60°$.

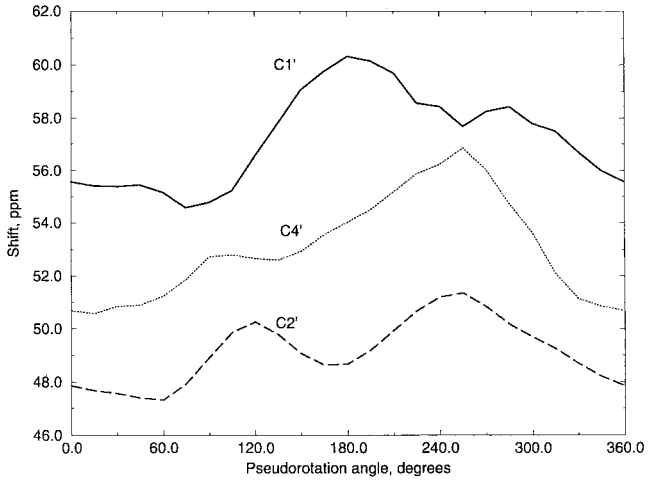

Figure 3. Calculated carbon chemical shifts for the model deoxyribose (Figure 1.1) as a function of the pseudorotation phase *P*. The chemical shift is obtained by subtracting the isotropic *deMon* shielding calculated from the reference isotropic shielding of 182.05 calculated for C in TMS. To get the three carbons on the same figure, an additional 60 ppm was subtracted from the C1′ shifts and 40 ppm subtracted from the C4′ shifts. The C2′ are not modified. The results presented are from the D1 set, with exocyclic torsions angles $\beta = \epsilon = 180°$; $\gamma = 60°$.

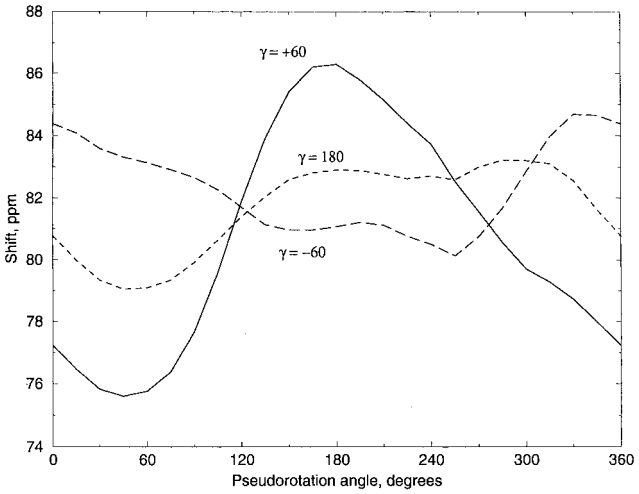

Figure 4. Calculated C3′ chemical shifts for the model deoxyribose (Figure 1.1) as a function of the pseudorotation phase *P*. The results presented correspond to the D1 set of structures, but with the exocyclic torsion angles β and ϵ rotated to 180°. The three conformers of γ are displayed in the figures: gauche ($\gamma = 60° \pm 15°$; unmodified values from D1 structures); trans (γ rotated to 180° for all structures), and −gauche (γ rotated to −60° for all structures). It can be seen that the results for $\gamma = 60° \pm 15°$ are almost identical to those presented in Figure 2 for the D1 set of structures, which have value of β and ϵ in the gauche region (60° ± 15°).

functional theory with a sum-over-states perturbation approach.[19] In this method, Kohn−Sham orbitals are inserted into a standard formula for chemical shielding,[34] and energy denominators are approximated by differences in Kohn−Sham orbital energies, corrected for changes in the exchange correlation potential that occur upon excitation. The gauge invariance requirement is treated using the individual gauge for localized orbitals (IGLO) approach.[35] Full details of the methods are given elsewhere.[19] The calculations used the IGLO-III basis set of Kutzelnigg and co-workers;[35] this is a relatively large basis set, with 11 s-type and 7 p-type Gaussians (contracted to 7s/6p) along with two uncontracted polarization functions for first row atoms (11s7p2d/7s6p2d) and 6 s-type Gaussians (contracted to 4s) along with two uncontracted polarization functions for H (6s2p/4s2p). All calculations used the Perdew−Wang-91 (PW91) exchange correlation potential[30] and the "Loc.1" correction for energy denominators.[19]

For all geometries, the proton and carbon shifts are reported relative to the computed shielding for TMS ($\sigma_H = 31.02$ ppm; $\sigma_C = 182.05$ ppm). The geometry of TMS was optimized at the BPW91/6-31G* level, and the shielding tensors were evaluated with the IGLO-III basis set as described above. ^{13}C chemical shift anisotropies were also evaluated from the computed shielding tensors. We computed the difference $\sigma_{orth} - \sigma_{par,}$ where σ_{par} is the shielding in the direction of the C−H bond and σ_{orth} is the average shielding orthogonal to this bond. This is the quantity that influences cross-correlation between dipolar and CSA relaxation pathways.[36]

3. Results

3.1. Methyl β-D-2-Deoxyribofuranoside. *3.1.a. Influence of the Sugar Conformation on the Calculated Chemical Shielding.* The calculated chemical shifts as a function of pseudorotation angle are displayed in Figures 2−4 (carbon shifts) and Figure 6 (proton shifts). It can clearly be seen that both carbon and hydrogen chemical shifts are affected by the pseudorotation of the deoxyribose. The differences in chemical shift between a representative C3′ endo (north; $P = 15°$) and C2′ endo (south; $P = 165°$) conformation of the deoxyribose are reported in Table 2 for different conformations of the exocyclic torsion angles. These differences are indicative of the magnitude of the shielding change with conformation.

The carbon most sensitive to the sugar repuckering is C3′ (Figure 2), which is more shielded in the N (C3′ endo) conformation than the S (C2′ endo) conformation by 10 ppm. C5′ is also significantly shielded in the N conformation, although the effect is smaller (5 vs 10 ppm). A similar trend has been reported experimentally (vide infra).[37] The variation in chemical shift observed for C1′, C2′, and C4′ (Figure 3) is less significant,

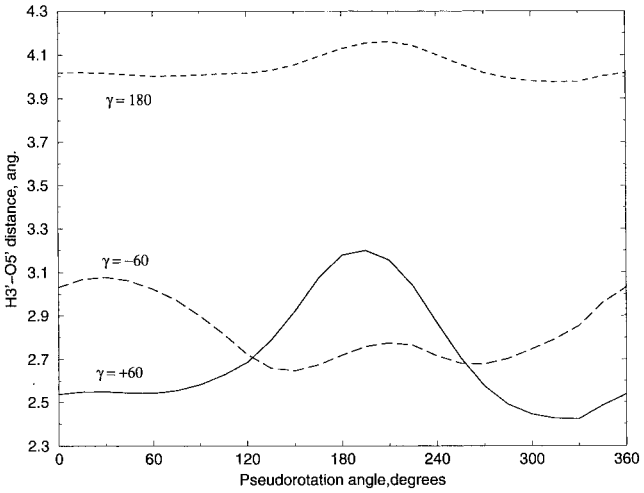

Figure 5. Distance between H3′ and O5′ in the model deoxyribose, as a function of the pseudorotation phase *P*. The results presented correspond to the D1 set of structures. The three conformers of γ are displayed in the figures: gauche ($\gamma = 60° \pm 15°$; unmodified values from D1 structures); trans (γ rotated to 180° for all structures), and −gauche (γ rotated to −60° for all structures).

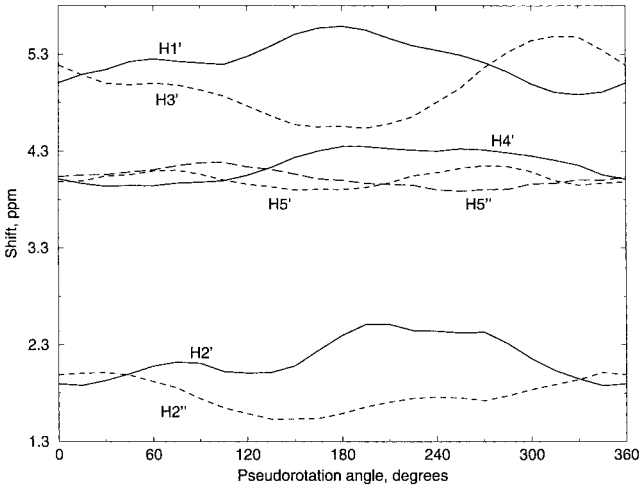

Figure 6. Calculated proton chemical shifts for the model deoxyribose (Figure 1.1) as a function of the pseudorotation phase *P*. The chemical shift is obtained by subtracting the isotropic *deMon* shielding calculated for the protons from the reference isotropic shielding of 31.02 calculated for H in TMS. The results presented are from the D1 (cf. Table 1) set of structures, with $\beta = \epsilon = 180°$; $\gamma = 60°$.

with a shielding increase of 3 ppm for C1′ and C4′ in the N conformation and 1 ppm for C2′. The general trend observed for the carbons in the model deoxyribose is thus an upfield shift in north conformations. These chemical shift trends are for the exocyclic dihedral angles $\beta = 180°$, $\epsilon = 180°$, and $\gamma = 60°$. As can be seen from Table 2, the upfield shift in north conformation is nearly independent of the value of the exocyclic torsions for C1′ and C4′ but is strongly correlated with the value of γ for C3′ and C5′. In Figure 4, we present a comparison of the variation of C3′ chemical shift with pseudorotation angle for three values of γ ($\gamma = 60°$, 180°, and −60°). The variation of C3′ chemical shift with pseudorotation and γ angles is strongly correlated with the distance between the H3′ and O5′ oxygen (cf. Figure 5), where short H3′−O5′ distances lead to an increased shielding of the C3′. These so-called steric effects on ^{13}C chemical shifts have been reported for a number of compounds.[37−39] They reflect van der Waals and/or charge polarization effects on ^{13}C chemical shifts.[39]

The results for the proton chemical shifts are presented in Figure 6. The general trend in the proton shifts is downfield in the N (C3′ endo) conformation with respect to the S (C2′ endo) conformation for H3′ and H2″ and upfield for H1′, H2′, and H4′ (with $\beta = 180°$; $\gamma = 60°$; $\epsilon = 180°$). H5′ and H5" are insensitive to the sugar repuckering. The data presented in Table 2 show that the upfield shift of H1′ and H4′ in N (C3′ endo) conformation is not sensitive to the value of the exocyclic torsions. The variations in shielding of H2′ and H2″, on the other hand, are sensitive to the exocyclic torsions. H3′ is the most sensitive to the sugar conformation. The downfield shift of H3′ in N conformation is observed only when $\gamma = +60°$ (cf. Table 2). The downfield shift of H3′ in N conformation can be related to the upfield shift of C3′, and both can be qualitatively understood as a polarization by O5′ in the direction H3′ δ^+ C3′ δ^-.

A recent analysis[60] of proton chemical shifts in DNA demonstrated that the ring current and magnetic anisotropy of the bases had an important influence on the ^{1}H shift. The results presented here indicate that the sugar conformation and the polarization effects linked to the backbone oxygens can also significantly influence the sugar proton shifts.

3.1.b. Comparison of Calculated and Experimental Chemical Shifts. In Figure 7 we present a comparison of calculated and experimental ^{13}C chemical shifts. The experimental data are from solid-state ^{13}C NMR study for crystalline nucleosides and nucleotides.[37] Although these experimental conditions differ from the isolated sugar used for the theoretical calculations of shifts, the correlation between experimental and calculated shifts is excellent. In particular, the upfield shift of C3′ and C5′ carbon in north conformation is clearly seen in both experimental and theoretical results. Figure 7 also shows a systematic difference (8.2 ppm) between calculated and observed ^{13}C shifts. C3′ and C5′ shifts in nucleosides, nucleotides, and nucleic acids are indeed observed at higher fields (i.e., C3′ between 65 and 75 ppm and C5′ between 55 and 66 ppm)[27] than what is calculated for the model deoxyribose (C3′ between 75 and 85 ppm and C5′ between 65 and 75 ppm).

In Figure 8, we present a comparison of the calculated and experimental proton chemical shifts for methyl 2′-deoxy-β-D-ribofuranoside. The experimental shifts have been measured in $CDCl_3$ at 292 K.[40] The calculated shifts assume an equimolar mixture of north and south conformers.[40] Figure 7 shows that the calculated shifts are in good agreement with the experimental ones.

3.1.c. Influence of ab Initio Method and Geometry Optimization. In Figure 2, we compare the chemical shifts calculated for C3′ with different sets of geometries for the deoxy sugar. The puckering amplitude τ_m for sets D2 and D3 is displayed as a function of pseudorotation angle in Figure 9. It can be seen that the maximum puckering amplitude varies significantly along the pseudorotation cycle, with $\tau_m = 40°$ for $P = 60$ and $\tau_m = 26°$ for $P = 188$. Variation in puckering amplitude as a function of pseudorotation has also been reported in ab initio studies of β-D-ribofuranose.[41] As can be seen from Figure 2, these variations in τ_m do not influence the chemical shielding. The D1 set of structures (with four dihedrals constrained and a constant puckering amplitude of 38°) indeed yields comparable results to the D2 set of structures (where only ν_3 is constrained and τ_m varies with P).

A significant difference is observed between shifts calculated with the D1 or D2 (BPW91/6-31G*) and D3 (HF/6-31G**) sets of structures: a systematic upfield shift is observed when the structures are obtained at the Hartree−Fock level. It is known

TABLE 2: Difference in Calculated Chemical Shift between North (C3′ Endo; $P = 15°$) and South (C2′ Endo; $P = 165°$) Conformations for Methyl 2′-Deoxy-β-D-ribofuranoside and for Deoxythymidine[a]

deoxyribose			$\Delta\delta$ (N − S) ppm[b]				
β	ϵ	γ	C1′	C2′	C3′	C4′	C5′
60	60	60	−3.4	0.6	−9.8	−3.2	−5.0
180	180	60	−4.4	−1.0	−10.2	−3.0	−5.1
180	180	180	−4.1	−0.5	−2.8	−3.8	0.6
180	180	−60	−2.6	1.4	3.1	−4.9	2.8

deoxythymidine			$\Delta\delta$ (N − S) ppm[b]				
β	ϵ	γ	C1′	C2′	C3′	C4′	C5′
180	180	60	1.1	3.1	−10.6	−1.6	−5.3

deoxyribose			$\Delta\delta$ (N − S) ppm[b]						
β	ϵ	γ	H1′	H2′	H2″	H3′	H4′	H5′	H5″
60	60	60	−0.28	0.13	−0.37	0.60	−0.67	0.12	0.10
180	180	60	−0.48	−0.37	0.47	0.53	−0.34	0.09	0.04
180	180	180	−0.52	0.14	0.41	0.02	−0.31	0.08	0.32
180	180	−60	−0.45	0.03	0.40	−0.25	−0.33	0.24	0.23

deoxythymidine			$\Delta\delta$ (N − S) ppm[b]						
β	ϵ	γ	H1′	H2′	H2″	H3′	H4′	H5′	H5″
180	180	60	−0.80	0.20	−0.15	0.23	−0.55	0.13	0.21

[a] D1 set of structures with various values of the exocyclic torsion angles β, ϵ, and γ. [b] These differences are taken between two frozen conformations, and they are indicative of the magnitude of the shielding change with conformation. Quantitative estimates of the change in shielding with conformation would require a more sophisticated treatment of conformational averaging effects.

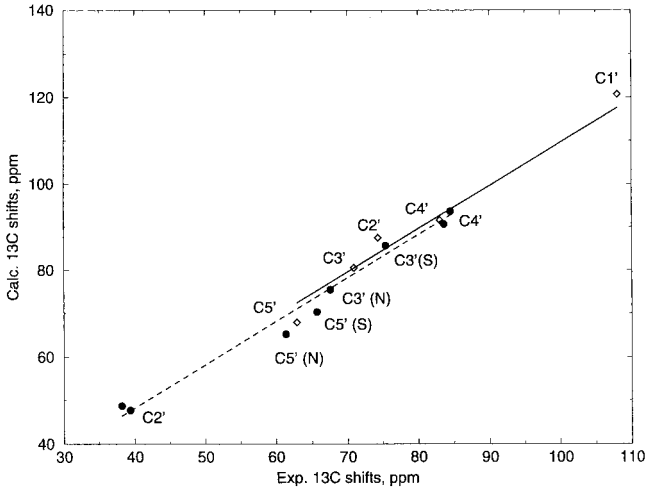

Figure 7. (filled symbols) Comparison of calculated and experimental carbon chemical shifts for the model deoxyribose (Figure 1.1). The experimental shifts for the north and south conformers are reported separately. The calculated shifts for the north conformer are from the D1 set of structures (BPW91/6-31G*) with $P = 15°$ and $\beta = \epsilon = 180°$, $\gamma = 60°$ and for the south conformer from D1 with $P = 165°$ and $\beta = \epsilon = 180°$, $\gamma = 60°$; they are given in ppm relative to the calculated value in TMS. The experimental values are from crystalline samples;[38] they are reported relative to external TMS. (open symbols) Comparison of calculated and experimental carbon chemical shifts for the model ribose (Figure 1.2). The calculated values assume an equimolar mixture of N and S conformers; they are given in ppm relative to the calculated value in TMS (the north conformer is from the R1 set of structures (BPW91/6-31G*) with $P = 0°$ and $\beta = \epsilon = 180°$; $\gamma = 60°$, and the South conformer is from R1 with $P = 150°$ and $\beta = \epsilon = 180°$ $\gamma = 60°$). The experimental values are from D_2O solutions;[43] they are reported relative to external TMS. The lines of slope 1 that best fit the data are also displayed on the figure.

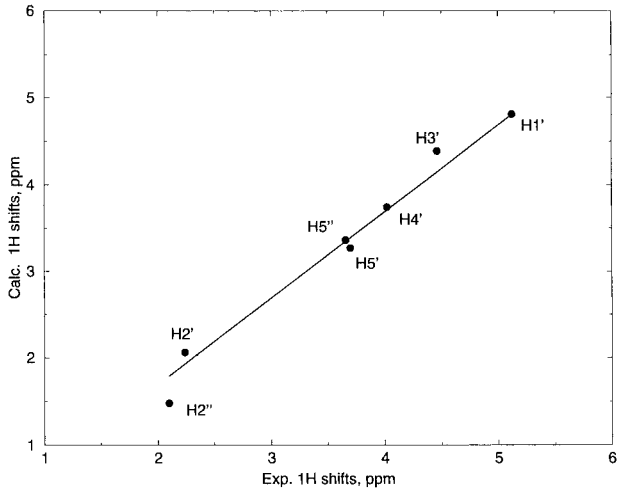

Figure 8. Comparison of calculated and experimental proton chemical shifts for the model deoxyribose (Figure 1.1). The calculated shifts are obtained from the fully optimized MP2/6-31G** structures (D5 set), assuming a 50−50 mixture of N and S conformers (i.e., calcd shift = 0.5 calcd shift (N) + 0.5 calcd shift (S)). They are given in ppm relative to the calculated value in TMS. The experimental values are from $CDCl_3$ solutions.[40]

that absolute values of carbon shieldings are sensitive to the quantum mechanical model.[23] The systematic trend observed here can be linked to the systematic increase in bond lengths observed between the HF and BPW91 geometries.[42] The different C−H bond lengths are between 1.10 and 1.11 Å in the BPW-91/6-31G* structures and between 1.08 and 1.09 Å in the HF/6-31G* structures. C−H bond lengths are thus systematically 0.02 Å shorter at the HF level. Likewise C−C lengths are 0.005 Å shorter and C−O lengths 0.025 Å shorter at the Hartree−Fock level, which leads to an increased electron density close to C and explains the increased shielding. The results obtained for the structures from the unconstrained geometry optimizations (D4 and D5 sets) are also displayed in Figure 2. The HF/6-31G** (D4 set) fully optimized structures give shifts extremely close to those obtained with the D3 sets of structures. Two sets of shifts are obtained for the D4 set, which corresponds to two values of the exocyclic β angle. As can be seen from Figure 2, the results are comparable for the

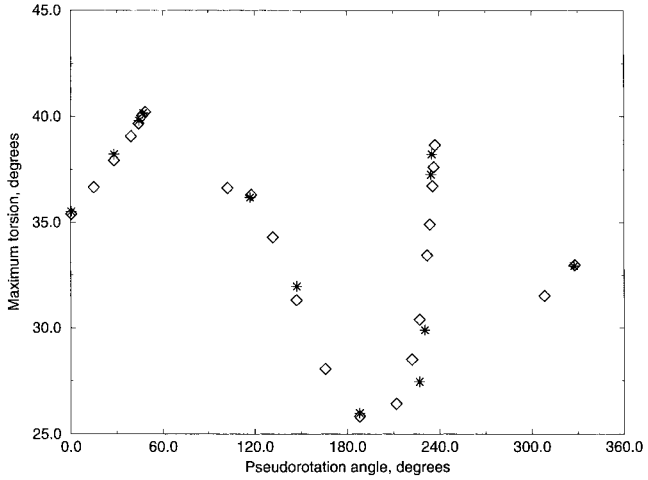

Figure 9. Maximum torsion τ_m as a function of the pseudorotation angle for the model deoxyribose. The results correspond to the D2 (*) and D3 (◇) sets of structures.

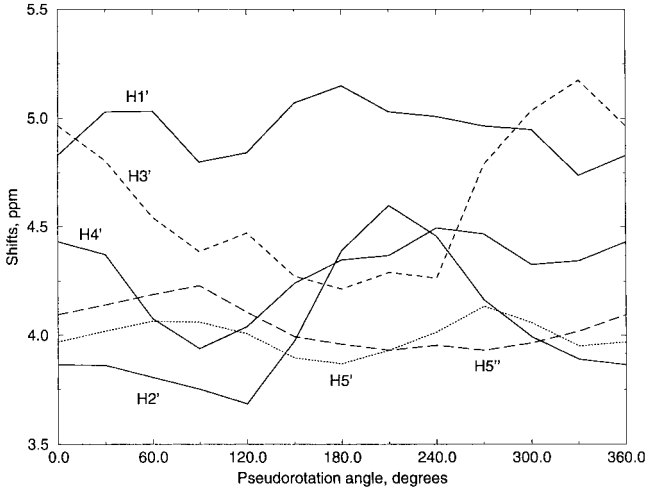

Figure 10. Calculated proton chemical shifts for the model ribose (Figure 1.2) as a function of the pseudorotation phase *P*. The chemical shift is obtained by subtracting the isotropic *deMon* shielding calculated for the protons from the reference isotropic shielding of 31.02 calculated for H in TMS. The results presented are from the R1 (cf. Table 1) set of structures, with $\beta = \epsilon = 180°$; $\gamma = 60°$.

two values of β. Finally, the shifts corresponding to the fully optimized MP2/6-31G** structures (D5 set) are intermediate between the HF and BPW91 sets of shifts, which can be related to general trends in bond lengths between the three methods. Hence, although absolute shieldings are quite sensitive to local geometry, the main conformational trends with torsion angles are preserved with various optimization strategies.

3.2. Methyl β-D-Ribofuranoside. *3.2.a. Influence of the Sugar Conformation on the Calculated Chemical Shielding.* Many of the features in the shifts for the ribose model mimic those seen in the deoxy model. The calculated chemical shifts as a function of pseudorotation angle are displayed in Figures 10 (proton shifts), 11, and 12 (carbon shifts). The differences in chemical shift between a representative C3′ endo (north; $P = 30°$) and C2′ endo (south; $P = 180°$) conformation of the ribose are reported in Table 3 for different conformations of the exocyclic torsion angles.

The chemical shift trends observed for the C3′, C4′, and C5′ ribose carbons are very similar to those observed for the deoxyribose, with a general upfield shift in N conformation. As for the deoxyribose, C3′ and C5′ are the most sensitive to

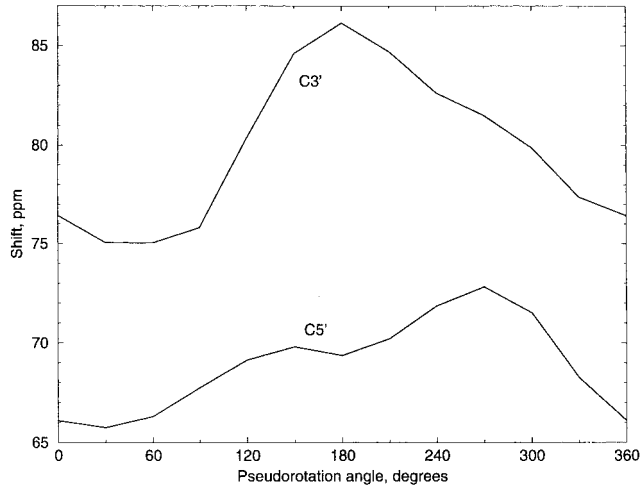

Figure 11. Calculated C3′ and C5′ chemical shifts for the model ribose (Figure 1.2) as a function of the pseudorotation phase *P*. The chemical shift is obtained by subtracting the isotropic *deMon* shielding calculated for C3′ and C5′ from the reference isotropic shielding of 182.05 calculated for C in TMS. The results presented are from the R1 (cf. Table 1) set of structures, with $\beta = \epsilon = 180°$; $\gamma = 60°$.

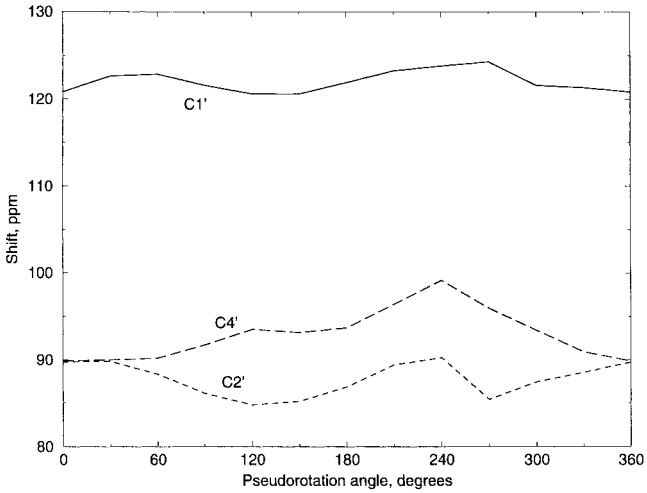

Figure 12. Calculated carbon chemical shifts for the model ribose (Figure 1.2) as a function of the pseudorotation phase *P*. The chemical shift is obtained by subtracting the isotropic *deMon* shielding calculated for C1′, C2′, and C4′ from the reference isotropic shielding of 182.05 calculated for C in TMS. The results presented are from the R1 (cf. Table 1) set of structures, with $\beta = \epsilon = 180°$; $\gamma = 60°$.

the sugar pucker with upfield shifts of 11 and 4 ppm in the N conformation, respectively. The absolute value of the C2′ shift is displaced downfield with respect to the deoxyribose, as expected. The variation of the C2′ and C1′ carbon shifts with the sugar conformation is different in the model ribose than in the model deoxyribose. The C2′ is deshielded by 3 ppm in the north conformation, and the C1′ is not affected much by pseudorotation, with a deshielding of 1 ppm in the north conformation.

The chemical shift dispersion of the ribose protons is reduced with respect to the model deoxyribose. The protons most affected by pseudorotation are H2′ and H3′ with a difference of 0.5 ppm between N and S conformations. These two protons move in opposite directions; i.e., H2′ moves upfield and H3′ downfield in C3′ endo. H1′ and H4′ are not affected much by pseudorotation, while H5′ and H5″ move downfield in C3′ endo.

3.2.b. Comparison of Calculated and Experimental Chemical Shifts. The carbon shifts of the model ribose have been published (in D_2O with external TMS as the ^{13}C shift refer-

TABLE 3: Difference in Calculated Chemical Shift between North (C3′ Endo; $P = 30°$) and South (C2′ Endo; $P = 180°$) Conformation for Methyl β-D-Ribofuranoside[a]

			$\Delta\delta$ (N − S) ppm[b]				
β	ϵ	γ	C1′	C2′	C3′	C4′	C5′
60	60	60	0.3	0.7	−10.9	−3.7	−3.9
180	180	60	0.8	2.9	−11.1	−3.7	−3.6
180	180	180	0.6	1.4	−3.6	−4.1	2.3
180	180	−60	3.4	−5.4	2.9	3.0	1.8

			$\Delta\delta$ (N − S) ppm[b]					
β	ϵ	γ	H1′	H2′	H3′	H4′	H5′	H5″
60	60	60	−0.12	−0.49	0.24	−0.46	0.21	0.23
180	180	60	−0.12	−0.53	0.59	0.02	0.15	0.18
180	180	180	−0.20	0.01	−0.06	0.08	0.42	−0.03
180	180	−60	0.28	0.07	0.04	−0.34	−0.11	−0.12

[a] D1 set of structures with various values of the exocyclic torsion angles β, ϵ, and γ. [b] Cf. footnote *b* from Table 2.

ence),[43] and in Figure 8 we present a comparison of the calculated and observed shifts. The correlation between calculated and observed shifts is good. As before there is a significant systematic difference between calculated and observed ^{13}C shifts (9.5 ppm). The calculated values are thus systematically deshielded by about 10 ppm with respect to the experimental ones, as was observed for the model deoxyribose. Other authors[19,61] have reported that DFT methods predict chemical shifts that are too deshielded as compared to experiment. They report mean errors of about 7 ppm[61] between calculated and experimental shifts, which is consistent with the results reported here. As can be seen from Figure 2, even if systematic differences exist between absolute values of chemical shifts calculated by different methods, the variation in chemical shift with sugar conformation, which is our main interest, is not affected by the choice of the quantum mechanical model.

It must also be noted that we have not corrected the calculated shieldings for effects such as rovibrational averaging, solvation, and bulk susceptibility.[44−46] Rovibrational averaging and solvation are generally thought to lower the shielding calculated in the gas phase at equilibrium geometry.[42,45] These effects should, however, cancel out to a large extent when computing shifts (with respect to TMS) as opposed to shielding.[45] It is also unlikely that these effects will affect selectively one conformation of the sugars over the others, so that the variation in sugar shift with conformation will remain largely unaffected.

Experimental studies of the temperature dependence of ^{13}C chemical shift in RNA oligomers[47,48] have been used to probe the effect of sugar conformation on ^{13}C shifts. Downfield shifts of C3′, C4′, and C5′ carbon resonances have been observed with increasing temperature. They were related to an increase in the population of the C2′ endo conformer with increasing temperature.[47,48] These experimental trends in shifts fully agree with the theoretical results. A downfield shift of C3′ in the C2′ endo conformation has also been observed in RNA structures. For example, in the UUCG loop of the P1 helix from group I self-splicing introns, the C3′ resonance of the central U and C are observed at 77.1 and 79.7 ppm while the C3′ resonance of other residues of the P1 helix are around 72 ppm.[49,50] These two residues are identified in C2′ endo conformation, contrary to the other residues which adopt the C3′ endo conformation most usually found in RNA structures.[49−52] Similar observations have been made in other tetraloop structures.[53]

C1′ resonances are generally observed to move upfield with increasing temperature while C2′ resonances are not affected much by temperature.[47,48] The C1′ resonances of the UUCG[49−52] and CUUG[53] loop nucleotides are also shifted upfield by about 5 ppm. The theoretical results presented here do not show large upfield shifts of C1′ in C2′ endo conformation. This was not observed in experimental studies on crystalline DNA oligonucleotides either.[37] Other structural parameters, such as, for example, the influence of the glycosidic torsion, will need to be considered to explain the C1′ shifts of the tetraloops.

TABLE 4: Calculated Chemical Shift Anisotropies ($\sigma_{orth} - \sigma_{para}$) in Representative North (C3′ Endo) and South (C2′ Endo) Conformation for Methyl 2′-Deoxy-β-D-ribofuranoside, Thymidine, and Methyl β-D-Ribofuranoside[a]

			$\sigma_{orth} - \sigma_{para}$ (N) ppm[b]			
β	ϵ	γ	C1′	C2′	C3′	C4′
			Deoxyribose			
60	60	60	32		58	27
180	180	60	32		54	33
180	180	180	33		52	33
180	180	−60	33		46	33
			Deoxythymidine			
180	180	60	33		61	28
			Ribose			
180	180	60	17	21	45	58

			$\sigma_{orth} - \sigma_{para}$ (S) ppm[b]			
β	ϵ	γ	C1′	C2′	C3′	C4′
			Deoxyribose			
60	60	60	51		28	21
180	180	60	49		26	27
180	180	180	51		33	28
180	180	−60	50		37	32
			Deoxythymidine			
180	180	60	58		34	18
			Ribose			
180	180	60	30	33	15	64

[a] D1 set of structures with various values of the exocyclic torsion angles β, ϵ, and γ. [b] For deoxyribose, the north conformation corresponds to $P = 15°$ and the south conformation to $P = 165°$. For thymidine and ribose, $P = 30°$ and $P = 180°$ are used for N and S.

3.3. Deoxythymidine. The differences in chemical shifts between a representative north (C3′ endo, $P = 15$) and south (C2′ endo, $P = 165$) conformation of the sugar in deoxythymidine are reported in Table 2. The variation in C3′ and C5′ chemical shift with the sugar pucker is very similar in deoxythymidine and in the isolated deoxyribose (upfield shift of 10.6 and 5.3 ppm for C3′ and C5′, respectively, in N conformation). C2′ experiences a downfield shift of 3.1 ppm in North conformation (versus 0.6 ppm in the isolated sugar) and C4′ an upfield shift of 1.6 ppm (versus 3.2 ppm in the isolated sugar). Not unexpectedly, the largest difference between methyl 2′-deoxy-β-D-ribofuranoside and deoxythymidine are observed for the C1′ carbon: a downfield shift of 1.1 ppm in N conformation is observed for deoxythymidine, while an upfield shift of 3.4 ppm was observed for the isolated sugar.

The variation of ^{1}H chemical shifts with the sugar pucker are affected by the presence of the thymine ring (cf. Table 2). The global trends observed for methyl 2′-deoxy-β-D-ribofuranoside are conserved for H3′, H5′, H5″ (downfield shift in N conformation) and H1′ (upfield shift in N conformation). H2′ and H2″, on the other hand, have their chemical shift trends reversed in the presence of the thymine ring (cf. Table 2).

3.4. Chemical Shift Anisotropies. There has been much recent interest in measuring chemical shift anisotropies (CSA).[36,54] Both experimental[36] and theoretical[55,56] studies of CSA on peptides and proteins have shown that small changes in isotropic

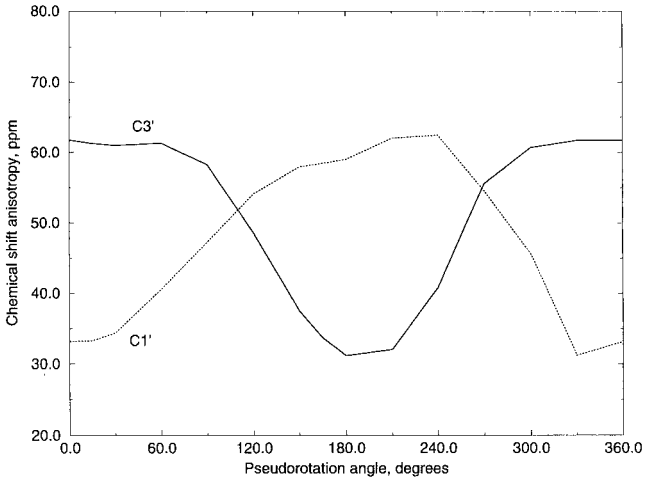

Figure 13. Chemical shift anisotropies ($\sigma_{orth} - \sigma_{para}$, ppm) for C1′ and C3′ carbons in deoxythymidine, as a function of pseudorotation angle. BPW91/6-31G* structures with $\beta = 180°$, $\epsilon = 60°$, $\gamma = 60°$, and $180° < \chi < 270°$.

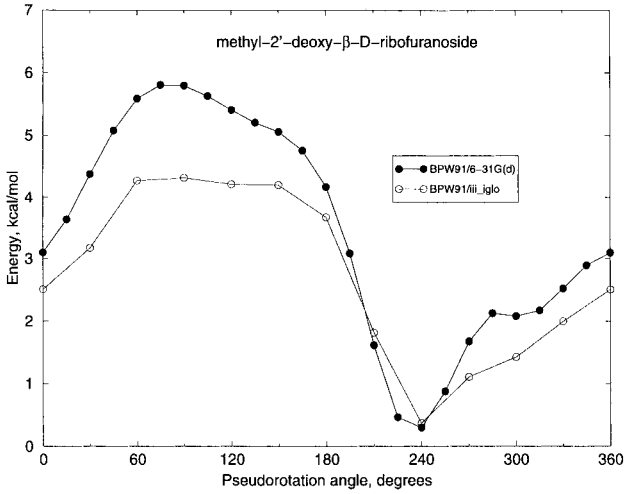

Figure 14. Relative energies of methyl-2′-deoxy-β-D-ribofuranoside as a function of pseudorotation angle. The results correspond to the D1 set of structures.

shift can be accompanied by much larger changes in chemical shift anisotropy. We examined the change in CSA with pseudorotation phase for the model deoxyribose, ribose, and deoxythymidine (cf. Table 4). As for the isotropic shift, the carbon most sensitive to pseudorotation is C3′ (cf. Figure 13). In the three systems studied, the CSA for the north conformation is 30 ppm larger than for the south conformation (with $\beta = \epsilon = 180°$ and $\gamma = 60°$). The trends in C3′ CSA are similar for the three values of γ ($\gamma = +60°$, 180°, and $-60°$), i.e., CSA(N) > CSA(S), but the differences between the north and south CSA's are reduced to 20 ppm for $\gamma = 180°$ and 10 ppm for $\gamma = -60°$. The CSA of C1′ is also substantially affected by the sugar conformation (cf. Figure 13), specially in the thymidine where CSA(N) is lower than CSA(S) by 25 ppm. The general trend observed for C1′ in the model sugars is also CSA(N) < CSA(S), but the difference is less pronounced.

4. Conclusion

In recent years, there has been a revival of interest in biomolecular chemical shifts and the structural information that can be obtained from them. Structural studies of nucleic acids by NMR often suffer from a scarcity of NOE restraints, and chemical shift information could potentially be useful in the structure determination process. Moreover, recent advances in isotope labeling of nucleic acid have made it possible to study ^{13}C- and ^{15}N-enriched RNA and DNA oligonucleotides, which will in turn significantly increase the amount of experimental chemical shift data available for nucleic acids.

In this paper we used density functional calculations to study the relationship between ribose and deoxyribose conformations and ^{13}C and ^{1}H chemical shifts. The influence of the sugar conformation on ^{13}C chemical shift anisotropies was also probed. Quantum chemical shielding calculations have recently begun to significantly advance our understanding of the relationship between structure and chemical shifts.[20,21,23] The quantum chemical approaches offer the opportunity to explore in detail not only local but also environmental shielding effects in a controlled manner.

The results presented here show that isotropic chemical shifts as well as shift anisotropies are strongly dependent on the sugar ring puckering and can therefore be very useful in determining the sugar preferred conformation. The calculated chemical shifts are in good agreement with the available experimental data, which further substantiates the use of quantum calculations in studying chemical shift trends in complex biomolecular systems.

TABLE 5: Relative Energies of the Minima and Transition States along the Pseudorotation Profile for Methyl 2′-Deoxy-β-D-ribofuranoside[a]

A.1.1. HF/6-31G** Methyl 2′-Deoxy-β-D-ribofuranoside

P	τ_m	β	γ	ΔE[b]
94.2	35.2	55.3	59.8	3.2
232.8	34.9	62.3	45.2	0.0
288.7	24.7	50.1	45.3	1.4
350.8	34.7	50.7	57.1	0.6
89.6	37.5	177.5	53.8	6.7
209.4	31.3	179.5	45.5	5.1
270.1	20.1	180.0	49.3	6.7
344.7	37.0	−178.3	56.6	3.3

A.1.2. MP2/6-31G** Methyl 2′-Deoxy-β-D-ribofuranoside

P	τ_m	β	γ	ΔE[c]
233.7	39.8	61.8	42.2	0
317.5	35.2	35.6	47.1	2.4

[a] Fully optimized structures. Units: degrees and kcal/mol. [b] Energy of the minimum: −533.638 915 075 Hartree [c] Energy of the minimum: −535.206 267 62 Hartree.

TABLE 6: Relative Energies of the Minima and Transition States along the Pseudorotation Profile for Methyl β-D-Ribofuranoside[a]

A.2.1. HF/6-31G** Methyl β-D-Ribofuranoside

P	τ_m	β	γ	ΔE[b]
87.8	39.6	56.0	60.0	3.1
155.7	36.2	62.5	59.2	0.1
282.7	26.9	53.4	44.9	2.1
359.8	35.9	53.4	57.8	0.0
87.6	40.4	180.0	54.0	6.4
155.7	37.2	165.6	48.5	2.8
259.2	20.1	180.0	47.7	7.3
349.5	37.1	180.0	55.9	2.3

A.2.2. HF/6-31G* β-D-Ribofuranose from ref 41

P	τ_m	β	γ	ΔE
90	42	180	180	3.7
162	35			2.4
270	30			4.4
342	38			0

[a] Fully optimized structures. Units: degrees and kcal/mol. [b] Energy of the minimum: −608.496 923 717 hartree.

TABLE 7: Comparison of Crystal and ab Initio Structures for Methyl β-D-Ribofuranose

distance (Å)	RHF/6-31G**	HF/6-31G* [a]	Xtal[a]
C1−C2	1.523		1.515
C2−C3	1.526	1.527	1.526
C3−C4	1.536	1.540	1.531
C4−O4	1.414	1.418	1.439
C1−O4	1.392	1.386	1.405
C1−O1	1.380	1.384	1.419
C2−O2	1.406	1.405	1.412
C3−O3	1.390	1.389	1.412
C5−05	1.400	1.400	1.421
C4−C5	1.513	1.512	1.502
angle // dihedral (deg)	**RHF/6-31G****	**HF/6-31G***	**Xtal**
C4−O4−C1	111.7	111.2	109.7
H1−C1−O1−CH3	64.6	55.9	58.0
H2−C2−O2−H	−48.5	−50.8	−29.9
H3−C3−O3−H	−160	−160.8	179.6
O5−C5−C4−C3 (γ)	56	−173.2	−176.0
C4−C5−O5−H (β)	180	−178.8	−174.6
C3−C4−O4−C1 (ν_4)	5.6	−3.4	−3.4
C2−C3−C4−O4 (ν_3)	−27	−20.2	−19.1
O1−C1−C2	107		107.5
C2−C3−O3	114.5		115.5
O2−C2−C3	106.5		109.0
O3−C3−C4	113.7		113.8
C1−C2−C3	101		101.3
C2−C3−C4	101.5		103.2
C1−C2−C3−H3	79.5		85.7
H1−C1−C2−C3	140.7		156.9
O1−C1−C2−O2	−161.5		160.6
O2−C2−C3−O3	−42.6		−40.6
H1−C1−C2−H2	86.7		−80.6
H2−C2−C3−H3	−40.5		−33.0

[a] From ref 41.

An analysis of conformational effects on proton chemical shifts in DNA has recently been published.[60] It was concluded that the bases have a dominant effect on the sugar proton shifts. Changes in chemical shifts of up to 2 ppm were reported as a function of the glycosidic torsion angle χ (for S sugars). The results presented here show that the sugar ring repuckering can modify proton shifts by up to 0.6 ppm and could therefore have a measurable effect on proton shifts.

The influence of the sugar repuckering on carbon shifts is significantly larger than that for ^{1}H, while the ring current/magnetic anisotropy of the bases will be of comparable magnitude for ^{1}H and ^{13}C. The carbon shifts correlation are thus large enough to provide useful sugar pucker information directly, even in the absence of a full analysis of other effects. The relatively good agreement with existing experimental data suggests that these calculations provide reliable insight into torsion angle effects in nucleic acid sugars. Further tests should be forthcoming as labeled samples become more routinely available.

Acknowledgment. This work was supported by NIH grant GM45811. The *deMon* density functional programs were kindly supplied by D. R. Salahub, V. G. Malkin, and O. L. Malkina. We thank Doree Sitkoff for many useful discussions during the course of this work. A.D. thanks Prof. J.-F. Lefevre and Prof. M. Karplus for their support of this work.

Appendix

Our principal focus in this paper has been on the dependence of shifts on torsion angles. Here we give some information about the computed energy profiles. Because the exocyclic torsion angles (especially β) differ between the model sugar and nucleic acid helices, we do not expect these energies to be especially relevant to nucleic acids, even though the shifts should be. Here we compare our energetics to experimental data in organic solvents and to other computational studies.

In Figure 14 the relative energies of methyl-2′-deoxy-β-D-ribofuranoside corresponding to the D1 set of structures are presented. The relative energies of the two minima and two transition states obtained for methyl-2′-deoxy-β-D-ribofuranoside are reported in Table 5.

It can be seen that for the deoxy compound, the minimum energy structures have pseudorotation phases P of 232.8° and 350.8° (HF/6-31G**), which is somewhat different from the C3′ endo (N) and C2′ endo (S) conformations in nucleic acids, where C3′ endo corresponds to $0° < P < 36°$ and C2′ endo to $144° < P < 190°$.[33] The conformational equilibrium of methyl-2′-deoxy-β-D-ribofuranoside in H_2O and $CDCl_3$ solutions has been studied by NMR.[40,58] It was concluded that in $CDCl_3$ the deoxy compound is in equilibrium between N and S conformers with a proportion of 50% N and 50% S. The pseudorotation parameters determined experimentally in CDCl3 solution[40] (P(north) = 340°; τ_m(north) = 45°; P(south) = 249°; τ_m(south) = 41°) are in good agreement with the theoretical gas-phase values obtained by full optimization at the MP2/6-31G** level (P(north) = 317°; τ_m(north) = 35°; P(south) = 234°; τ_m(south) = 40°).

By comparison, the pseudorotation parameters for the minimum energy conformation of methyl-β-D-ribofuranose are closer to those observed in nucleosides and nucleotides (cf. Table 5). Ab initio geometry optimization of β-D-ribofuranose and methyl-β-D-ribofuranose at the HF/6-31G* and MP2/6-31G* level have recently been published.[41] The energy profile reported for β-D-ribofuranose (at HF/6-31G*) as a function of pseudorotation angle shows that $P = -18°$ (C3′ endo) is the global minimum. The C2′ endo conformer ($P = 162°$) is a local minimum, 2.4 kcal/mol higher than the global one. The east barrier ($P = 90°$) is 3.7 kcal/mol, and the west barrier ($P = 270°$) is 4.4 kcal/mol.[41] These results are in general agreement with those reported in Table 6 for methyl-β-D-ribofuranose. A different choice of the values of the exocyclic torsion angles and the addition of the methyl group in our model ribose are most likely responsible for the difference in the energy profile between the two riboses. An ab initio and a crystal structure of methyl-β-D-ribofuranose in a north conformation have also been reported.[41] These data are compared with ours in Table 7

References and Notes

(1) Pardi, A.; Wagner, G.; Wüthrich, K. *Eur. J. Biochem.* **1983,** *137*, 445.
(2) Szilagyi, L.; Jardetzky, O. *J. Magn. Reson.* **1989,** *83*, 441.
(3) Pastore, A.; Saudek, V. *J. Magn. Reson.* **1990,** *90*, 165.
(4) Spera, S.; Bax, A. *J. Am. Chem. Soc.* **1991,** *113*, 5490.
(5) Wishart, D. S.; Sykes, B. D.; Richards, F. M. *J. Mol. Biol.* **1991,** *222*, 311.
(6) Wishart, D. S.; Sykes, B. D.; Richards, F. M. *Biochemistry* **1992,** *31*, 1647.
(7) Wishart, D. S.; Sykes, B. D. *J. Biomol. NMR* **1994,** *4*, 171.
(8) Ösapay, K.; Case, D. A. *J. Biomol. NMR* **1994,** *4*, 215.
(9) Ösapay, C.; Case, D. A. *J. Am. Chem. Soc.* **1991,** *113*, 9436.
(10) Asakura, T.; Taoka, K.; Demura, M.; Williamson, M. P. *J. Biomol. NMR* **1995,** *6*, 227.
(11) Williamson, M. P.; Asakura, T.; Nakamura, E.; Demura, M. *J. Biomol. NMR* **1992,** *2*, 83.
(12) Williamson, M. P.; Asakura, T. *J. Magn. Reson.* **1993,** *101*, 63.
(13) Le, H. B.; Pearson, J. G.; de Dios, A. C.; Oldfield, E. *J. Am. Chem. Soc.* **1995,** *117*, 3800.
(14) Oldfield, E. *J. Biomol. NMR* **1995,** *5*, 217.
(15) Sulzbach, H. M.; Schleyer, P. V. R.; Schaefer, H. F. I. *J. Am. Chem. Soc.* **1994,** *116*, 3967.

(16) Sulzbach, H. M.; Schleyer, P. V. R.; Schaefer, H. F. *J. Am. Chem. Soc.* **1995,** *117*, 2632.
(17) Jiao, D.; Barfield, M.; Hruby, V. J. *J. Am. Chem. Soc.* **1993,** *115*, 10883.
(18) Chesnut, D. B.; Phung, C. G. In *Nuclear Magnetic Shieldings and Molecular Structure*; Tossell, J. A., Ed.; Kluwer Academic Publishers: Dordrecht, 1993.
(19) Malkin, V. G.; Malkina, O. L.; Casida, M. E.; Salahub, D. R. *J. Am. Chem. Soc.* **1994,** *116*, 5898.
(20) Pearson, J. G.; Wang, J. F.; Markley, J. L.; Le, H.; Oldfield, E. *J. Am. Chem. Soc.* **1995,** *117*, 8823.
(21) de Dios, A. C.; Oldfield, E. *J. Am. Chem. Soc.* **1994,** *116*, 5307.
(22) Sulzbach, H. M.; Vacek, G.; Shreiner, P. R.; Galbraith, J. M.; Schleyer, P. v. R.; Schaefer, H. F. I. *J. Comput. Chem.* **1997,** *18*, 126.
(23) Case, D. A. *J. Biomol. NMR* **1995,** *6*, 341.
(24) Giessner-Prettre, C.; Pullman, B. *Q. Rev. Biophys.* **1987,** *20*, 113.
(25) van de Ven, F. J. M.; Hilbers, C. W. *Eur. J. Biochem.* **1988,** *178*, 1.
(26) van de Ven, F. J. M.; Hilbers, C. W. *Nucleic Acids Res.* **1988,** *16*, 5713.
(27) Wijmenga, S. S.; Mooren, M. M. W.; Hilbers, C. W. In *NMR of nucleic acids; from spectrum to structure*; Roberts, G. C. K., Ed.; Oxford University Press: Oxford, 1993.
(28) Frisch, M. J.; Trucks, G. W.; Schlegel, H. B.; Gill, P. M. W.; Johnson, B. G.; Robb, M. A.; Cheeseman, J. R.; Keith, T.; Petersson, G. A.; Montgomery, J. A.; Raghavachari, K.; Al-Laham, M. A.; Zakrzewski, V. G.; Ortiz, J. V.; Foresman, J. B.; Cioslowski, J.; Stefanov, B. B.; Nanayakkara, A.; Challacombe, M.; Pen, C. Y.; Ayala, P. Y.; Chen, W.; Wong, M. W.; Andres, J. L.; Replogle, E. S.; Gomperts, R.; Martin, R. L.; Fox, D. J.; Binkley, J. S.; Defrees, D. J.; Baker, J.; Stewart, J. P.; Head-Gordon, M.; Gonzalez, C.; Pople, J. A. *Gaussian 94* Revision C.3; Gaussian, Inc.: Pittsburgh, PA, 1994.
(29) Becke, A. D. *Phys. Rev. A.* **1988,** *38*, 3098.
(30) Perdew, J. P.; Wang, Y. *Phys. Rev. B* **1992,** *45*, 13244.
(31) Hehre, W. J.; Radom, L.; Schelyer, P. v. R.; Pople, J. A. *Molecular Orbital Theory*; John Wiley: New York, 1986.
(32) Saenger, W. *Principles of Nucleic Acid Structure*; Springer-Verlag: New York, 1983.
(33) Gelbin, A.; Schneider, B.; Clowney, L.; Hsieh, S.-H.; Olson, W. K.; Berman, H. M. *J. Am. Chem. Soc.* **1996,** *118*, 519.
(34) Ramsey, N. F. *Phys. Rev.* **1950,** *78*, 699.
(35) Kutzelnigg, W.; Fleischer, U.; Schindler, M. *NMR, Basic Principles and Progress*; Springer-Verlag: New York, 1990.
(36) Tjandra, N.; Bax, A. *J. Am. Chem. Soc.* **1997,** *119*, 9576.
(37) Santos, R. A.; Tang, P.; Harbison, G. S. *Biochemistry* **1989,** *28*, 9372.
(38) Harbison, G. S.; Smith, S. O.; Pardoen, J. A.; Courtin, J. M. L.; Lugtenburg, J.; Herzfeld, J.; Mathies, R. A.; Griffin, R. G. *Biochemistry* **1985,** *24*, 6955.
(39) Sitkoff, D.; Case, D. A. *J. Am. Chem. Soc.* **1997**, *119*, 12262.
(40) Raap, J.; van Boom, J. H.; van Lieshout, H. C.; Haasnoot, C. A. G. *J. Am. Chem. Soc.* **1988,** *110*, 2736.
(41) Podlasek, C. A.; Stripe, W. A.; Carmichael, I.; Shang, M.; Basu, B.; Serianni, A. S. *J. Am. Chem. Soc.* **1996,** *118*, 1413.
(42) Chesnut, D. B. *Rev. Comput. Chem.* **1996,** *8*, 246.
(43) Ritchie, R. G. S.; Cyr, N.; Korsch, B.; Koch, H. J.; Perlin, A. S. *Can. J. Chem.* **1975,** *53*, 1424.
(44) Jameson, C. J. *J. Chem. Phys.* **1977,** *66*, 4977.
(45) Jameson, A. K.; Jameson, C. J. *Chem. Phys. Lett.* **1987,** *134*, 461.
(46) Jameson, C. J. *Chem. Rev.* **1991,** *91*, 1375.
(47) Lankhorst, P. P.; Erkelens, C.; Haasnoot, C. A. G.; Altona, C. *Nucleic Acids Res.* **1983,** *11*, 7215.
(48) Stone, M. P.; Winkle, S. A.; Borer, P. N. *J. Biomol. Struct. Dyn.* **1986,** *3*, 767.
(49) Allain, F. H. T.; Varani, G. *J. Mol. Biol.* **1995,** *250*, 333.
(50) Allain, F. H. T.; Varani, G. *Nucleic Acids Res.* **1995,** *23*, 341.
(51) Varani, G.; Tinoco, I. *J. Am. Chem. Soc.* **1991,** *113*, 9349.
(52) Cheong, C.; Varani, G.; Tinoco, I. *Nature* **1990,** *346*, 680.
(53) Jucker, F. M.; Pardi, A. *Biochemistry* **1995,** *34*, 14416.
(54) Tjandra, N.; Szabo, A.; Bax, A. *J. Am. Chem. Soc.* **1996,** *118*, 6986.
(55) Havlin, R. H.; Le, H.; Laws, D. D.; deDios, A. C.; Oldfield, E. *J. Am. Chem. Soc.* **1997,** *119*, 11951.
(56) Walling, A. E.; Pargas, R. E.; de Dios, A. C. *J. Phys. Chem. A* **1997,** *101*, 7299.
(57) Sitkoff, D.; Case, D. A. *Prog. Nucl. Magn. Reson. Spectrosc.*, in press.
(58) Gerlt, J. A.; Youngblood, A. V. *J. Am. Chem. Soc.* **1980,** *102*, 7433.
(59) Frisch, M. J.; Frisch, A.; Foresman, J. B. *Gaussian 94 user's reference*; Gaussian, Inc.: Pittsburgh, PA, 1994.
(60) Wijmenga, S. S.; Kruithof, M.; Hilbers, C. W. *J. Biomol. NMR* **1997**, *10*, 337.
(61) Cheeseman, J. R.; Trucks G. W.; Keith T. A. Frisch M. J. *J. Chem. Phys.* **1996** *104*, 5497.